Briefing Space Weather

2022/09/20

1 Sun

1.1 Responsible: José Cecatto

09/12 – M1.8 flare; Fast wind stream (=<450 km/s); 1 CME c.h.c. toward the Earth;
09/13 – No flare (M/X); No fast wind stream; 3 CME c.h.c. toward the Earth;
09/14 – M1.1 flare; No fast wind stream; 2 CME c.h.c. toward the Earth;
09/15 – No flare (M/X); No fast wind stream; 3 CME c.h.c. toward the Earth;
09/16 – M7.9, M6.2 flares; No fast wind stream; 7 CME c.h.c. toward the Earth;
09/17 – M1.9, M2.6 flares; No fast wind stream; 4 CME c.h.c. toward the Earth;
09/18 – No flare (M/X); Fast wind stream (=< 550 km/s); 6 CME c.h.c. toward the Earth;
09/19 – No flare (M/X); Fast wind stream (=< 550 km/s); 2 CME c.h.c. toward the Earth;
Prev.: Fast wind stream expected up to the day 19 and, on September 22-23; for the next 2 days (20% M, 05% X)
probability of M / X flares; also, occasionally other CME can present component toward the Earth.
c.h.c. – can have a component; * partial halo; ** halo

2 Sun

2.1 Responsible: Douglas Silva

- WSA-ENLIL (Prediction for CME : 022-09-09T07:24Z))
  - The simulation results indicate that the flank of CME will reach the DSCOVR mission between 2022-09-13T14:00Z and 2022-09-14T04:00Z.
- WSA-ENLIL (Prediction for CME : 2022-09-16T02:00Z)
  - The simulation results indicate that the flank of CME will reach the DSCOVR mission between 2022-09-18T19:00Z and 2022-09-19T09:00Z.

Coronal holes (SPOCA):

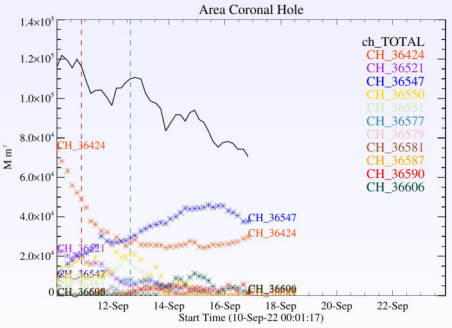

Figura: The solid line in black shows the products of the sum of areas for each detection interval performed by SPOCA between September 10 and 17, 2022.

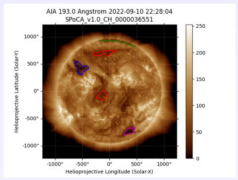

Figura: Above the 193 Å image of the Sun are highlighted coronal holes observed by SPOCA around 22:28 UT on September 10, 2022 (red dot line).

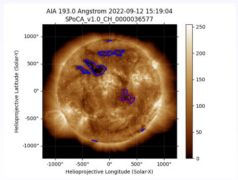

Figura: Above the 193 Å image of the Sun are highlighted coronal holes observed by SPOCA around 15:19 UT on September 12, 2022 (blue

WSA - ENLIL and SPOCA

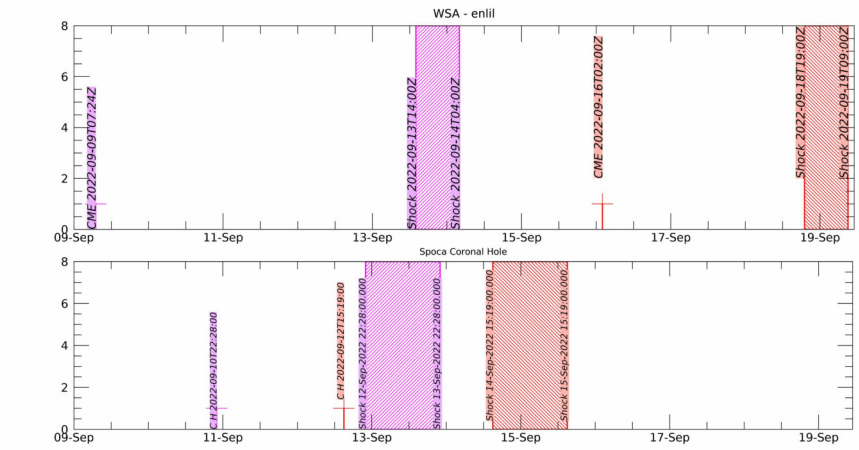

3 Interplanetary Medium

3.1 Responsible: Paulo Jauer

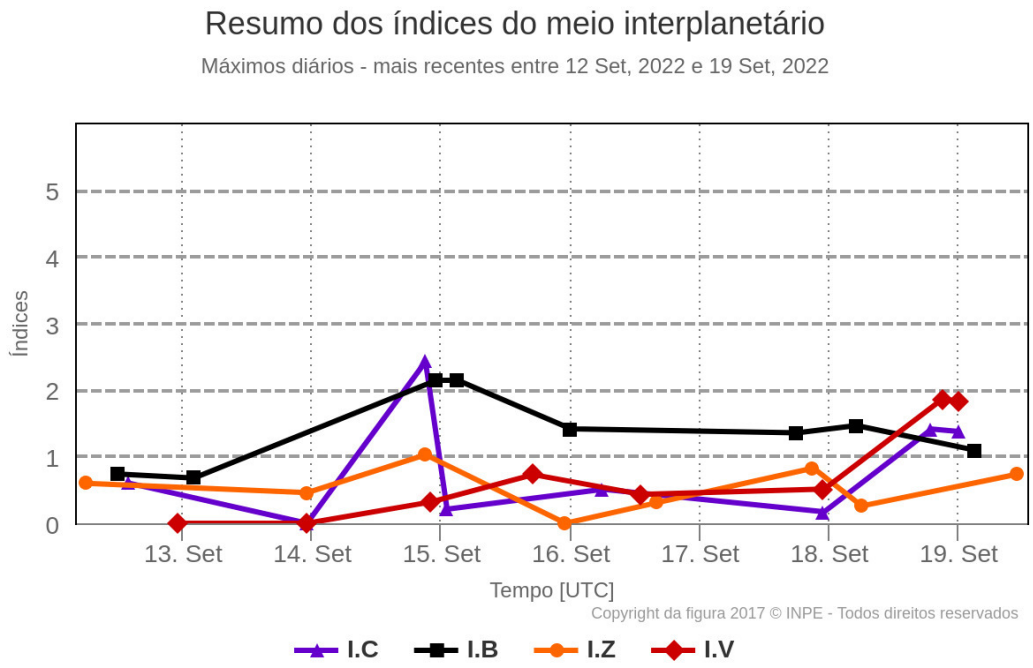

- The interplanetary medium region in the last week showed a low/moderate level of plasma perturbations due to the possible interaction of CME and HSS-like structures identified by the DISCOVR satellite in the interplanetary medium.
- The modulus of the interplanetary magnetic field component peaked at 15 nT on 15/Sep at 03:30 during the analyzed period.
- The BxBy components showed variations in the analyzed period, both remaining oscillating within the [+15, -15] nT interval, with the presence of a sector change on Sep/15 at 1:30 pm.
- The component of the bz field had a minimum value on 14/Sep 21:30 UT of -6nT and maximum positive value of 15/Sep 11:30 UT 12.5nT.
- The density of the solar wind showed a peak on 14/Sep 15:30 of 51 p/cm^3.
- The solar wind speed remained mostly below 400 km/s during the analyzed period.
- The magnetopause position was oscillating with a minimum value recorded on September 14 at 20:30 UT of 7.9 Re.

4 Radiation Belts

4.1 Responsible: Ligia Alves da Silva

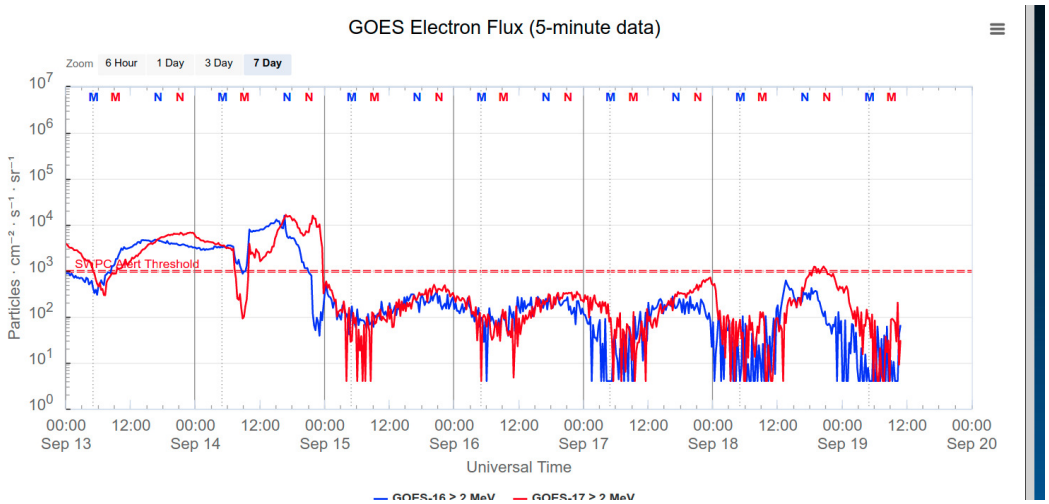

Figura 1: High-energy electron flux (> 2MeV) obtained from GOES-16 and GOES-17 satellite. Source: `https://www.swpc.noaa.gov/products/goes-electron-flux`

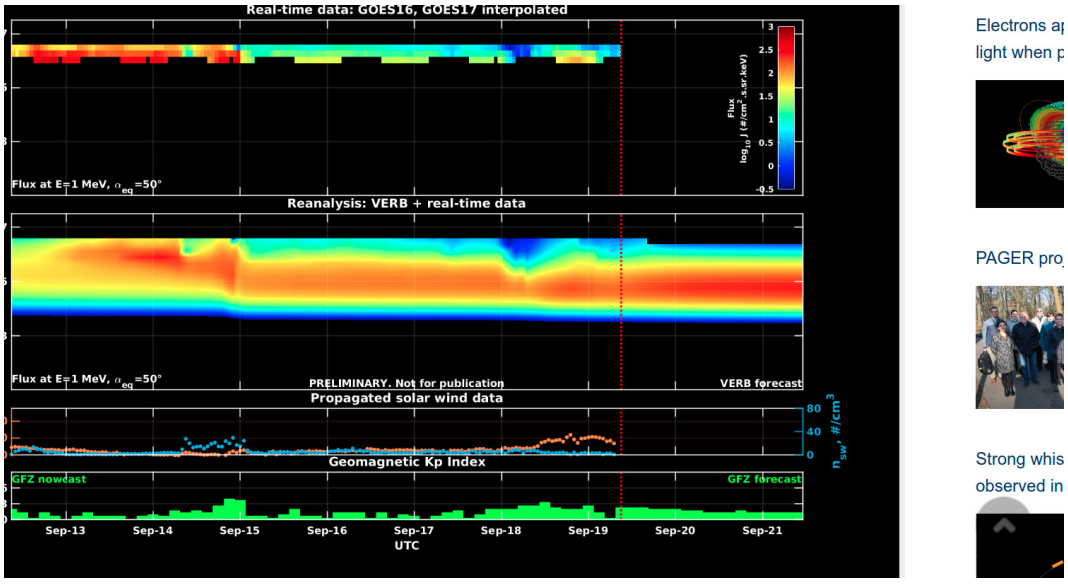

Figura 2: high-energy electron flux data (real-time and interpolated) obtained from GOES-16 and GOES-17 satellites. Reanalysis's data from VERB code and interpolated electron flux. Solar wind velocity and proton density data from ACE satellite. Source: `https://rbm.epss.ucla.edu/realtime-forecast/`

High-energy electron flux (> 2 MeV) in the outer boundary of the outer radiation belt obtained from geostationary satellite data GOES-16 and GOES-17 (Figure 1) hows significant variability during the analyzed period. The first electron flux increase is configured as a rapid dropout, being observed at 08:45 UT on September 14th. The second dropout confines the electron flux below 10^3 partículas/$(cm^2 ssr)$ for approximately three days, followed by a slight electron flux increase reaching the value of 10^3 partículas/$(cm^2 ssr)$ on September 17th. A new electron flux increase was observed exceeding the value of 10^3 partículas/$(cm^2 ssr)$ on September 18th.

The GOES-16 and GOES-17 satellite data are interpolated and assimilated into the VERB code (Figure 2), which reconstructs this electron flux considering the Ultra Low Frequency (ULF) waves'

radial diffusion. The simulation (VERB code) shows that the first two dropouts were confined at the outer boundary of the outer radiation belt ($L - shell > 6$ RE). On the other hand, the dropout that precedes the last enhancement hits more internal L-shells. These electron flux variabilities coincide with the arrival of solar wind structures and ULF wave activities.

5 ULF waves

5.1 Responsible: Graziela B. D. Silva

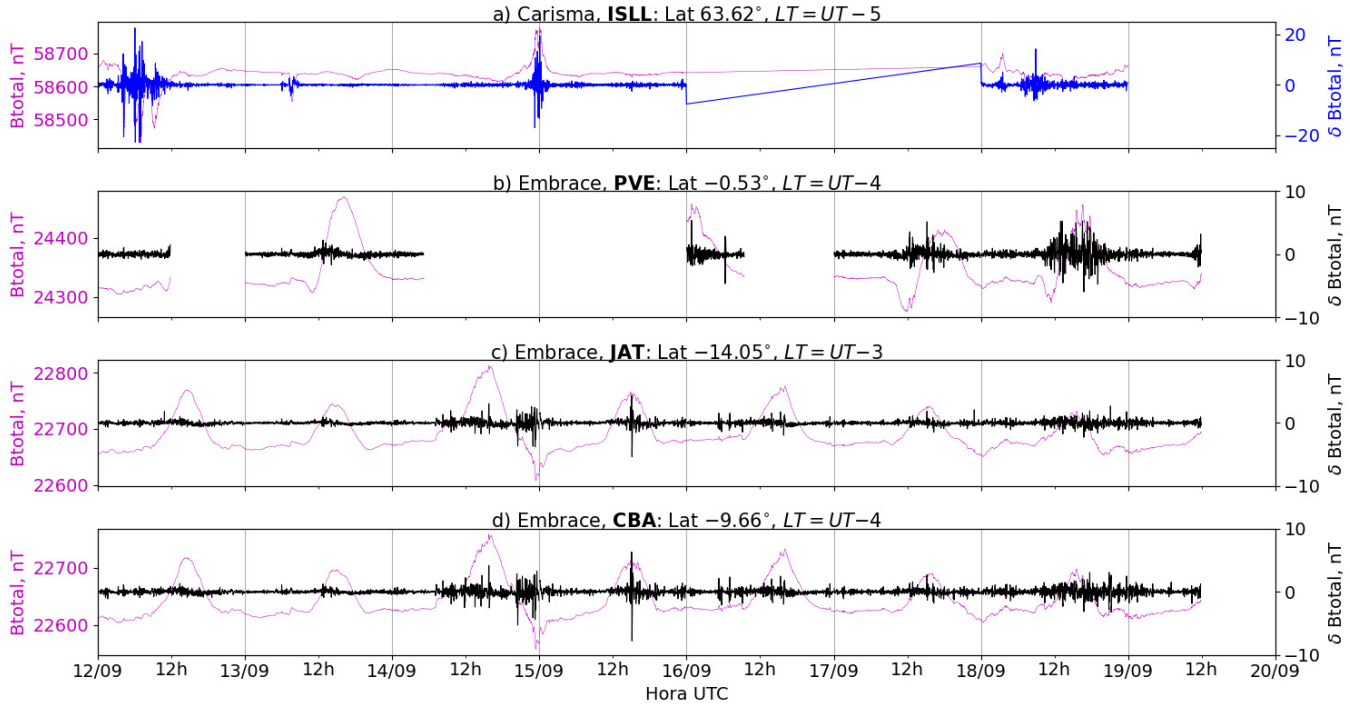

Figura 3: a) Timeseries of the geomagnetic field total component measured at ISLL station (Island Lake) of the CARISMA magnetometer network in magenta, along with the associated perturbation in the Pc5 band shown in blue. b-d) timeseries of the geomagnetic field total component measured at stations PVE (Porto Velho), JAT (Jataí), and CBA (Cuiabá) of the EMBRACE network in magenta, along with the Pc5 perturbation in blue.

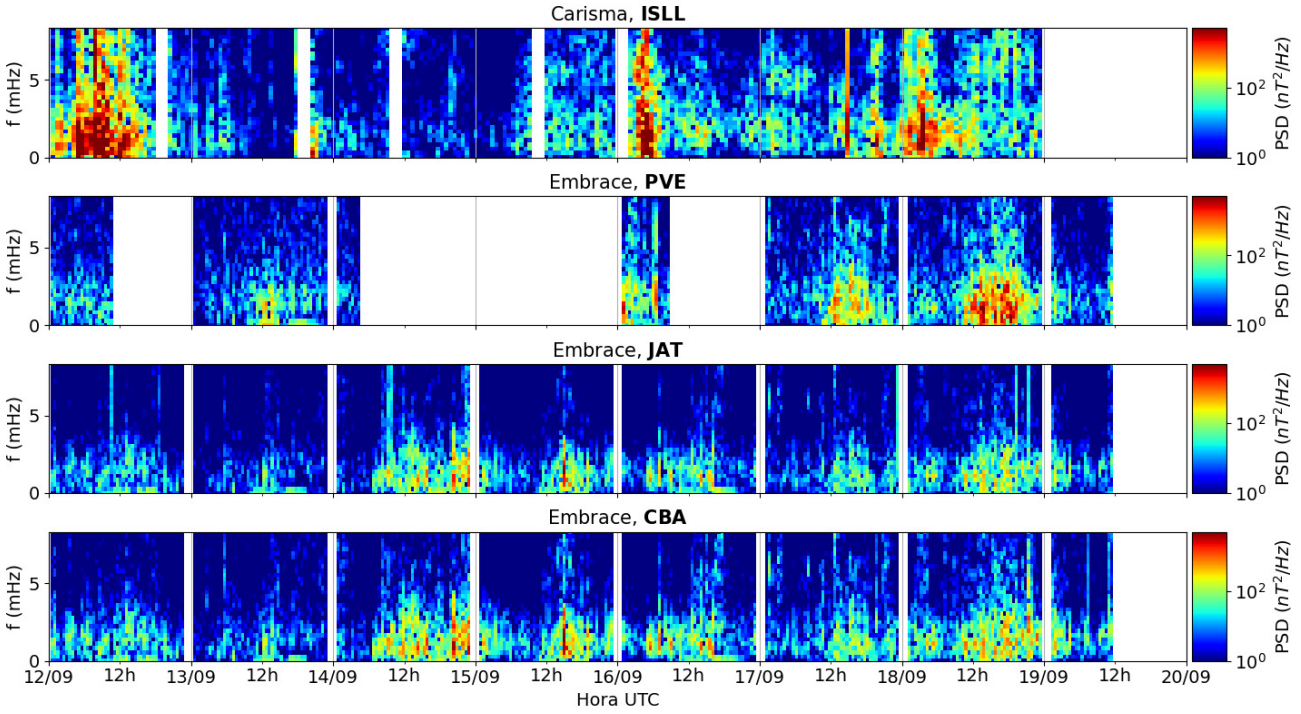

Figura 4: a-d) Time evolution of the power spectral density obtained from the filtered timeseries of the geomagnetic field total component (δ Btotal) for a) the high latitude station (ISLL-CARISMA), and b-d) for the low latitude stations of EMBRACE (PVE, JAT, CBA).

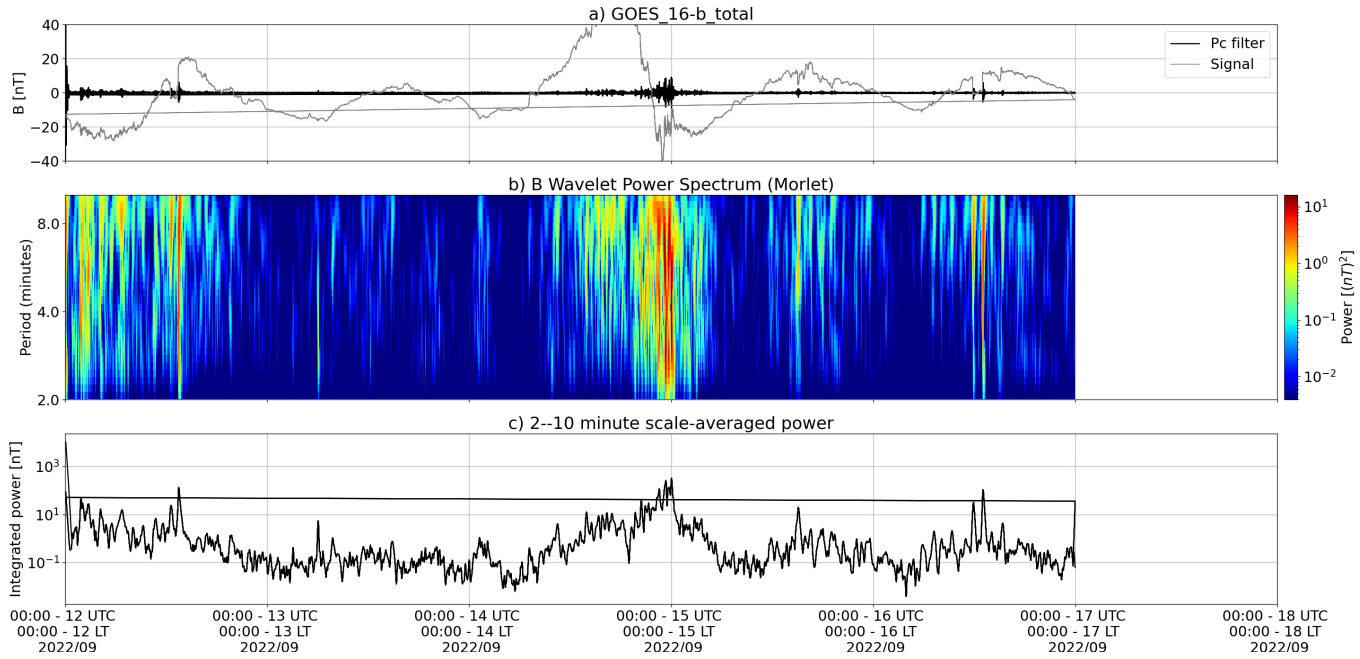

Figura 5: a) Timeseries of the geomagnetic field total component measured by GOES 16, together with the Pc5 fluctuation in black. b) Wavelet power spectrum of the filtered timeseries. c) Average ULF power in the period range from 2 to 10 minutes.

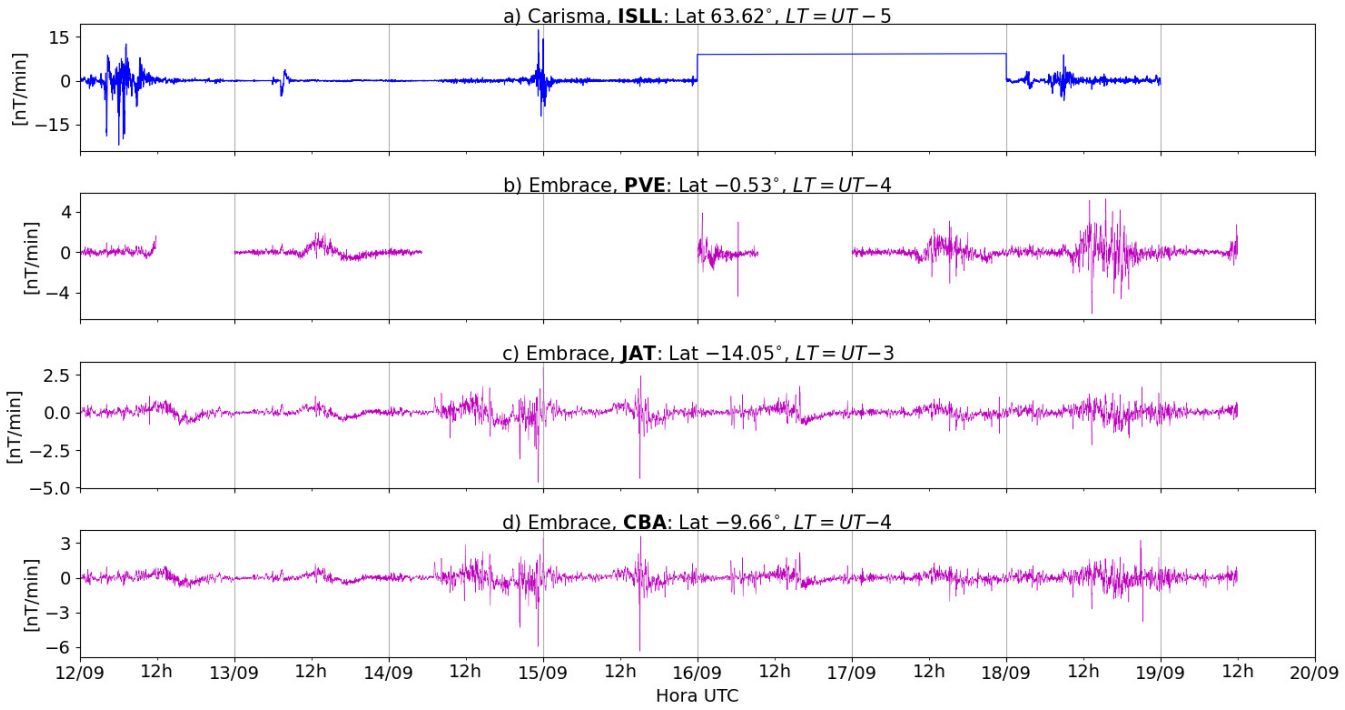

Figura 6: a-d) Rate of change of the geomagnetic field total component (dB/dt) obtained for a) the high latitude station (ISLL-CARISMA), and b-d) for the low latitude stations of EMBRACE (PVE, JAT, CBA).

- The GOES 16 satellite in geosynchronous orbit (L $\sim$ 6.6) registered significant activity of Pc5 ULF waves on September 12 and on Sep. 14 through Sep. 15. This last activity was associated with a compression followed by decrease in the total component of the geomagnetic field measured in situ by the spacecraft.
- As observed on the ground, the ISLL station of the Carisma network (high latitude, L=5.15) registered ULF wave activity Sep. 12, 14 and 18, despite that the amplitude levels of the field fluctuations did not surpassed the interval [-25,+25] nT.
- The low latitude stations of Embrace registered moderate to intense levels of ULF wave activity (i.e., δB in the interval of $\sim$ [-5,+5] nT) as of Sep. 14, showing strong influence of the Equatorial electrojet on the wave activity observed at PVE station.
- There were peaked and prolonged dB/dt signals simultaneously observed at the low latitudes over Brazil on Sep. 14 (starting at $\sim$ 9 UT), Sep. 15 (after 12 UT) and on Sep. 18 (after 12 UT). However, such dB/dt occurrences have not been overall correlated with those registered at ISLL station.

6 Geomagnetic activity

6.1 Responsible: Lívia Alves

In the week of September 13-19, the following events related to geomagnetic activity stand out:

- The data from the Embrace magnetometer network registered instabilities on Sep. 14 and 18.
- On Sep. 14, the magnetometers of the Embrace network recorded a drop to values of -80 nT in the H component.
- The geomagnetic field was active, the AE index was at 500 nT for several hours on Sep. 19. The Dst index reached -32 nT (Sep. 14). The highest Kp of the week was 4o.

- The geomagnetic field measured at the GOES orbit shows instabilities on Sep. 14 and 19.

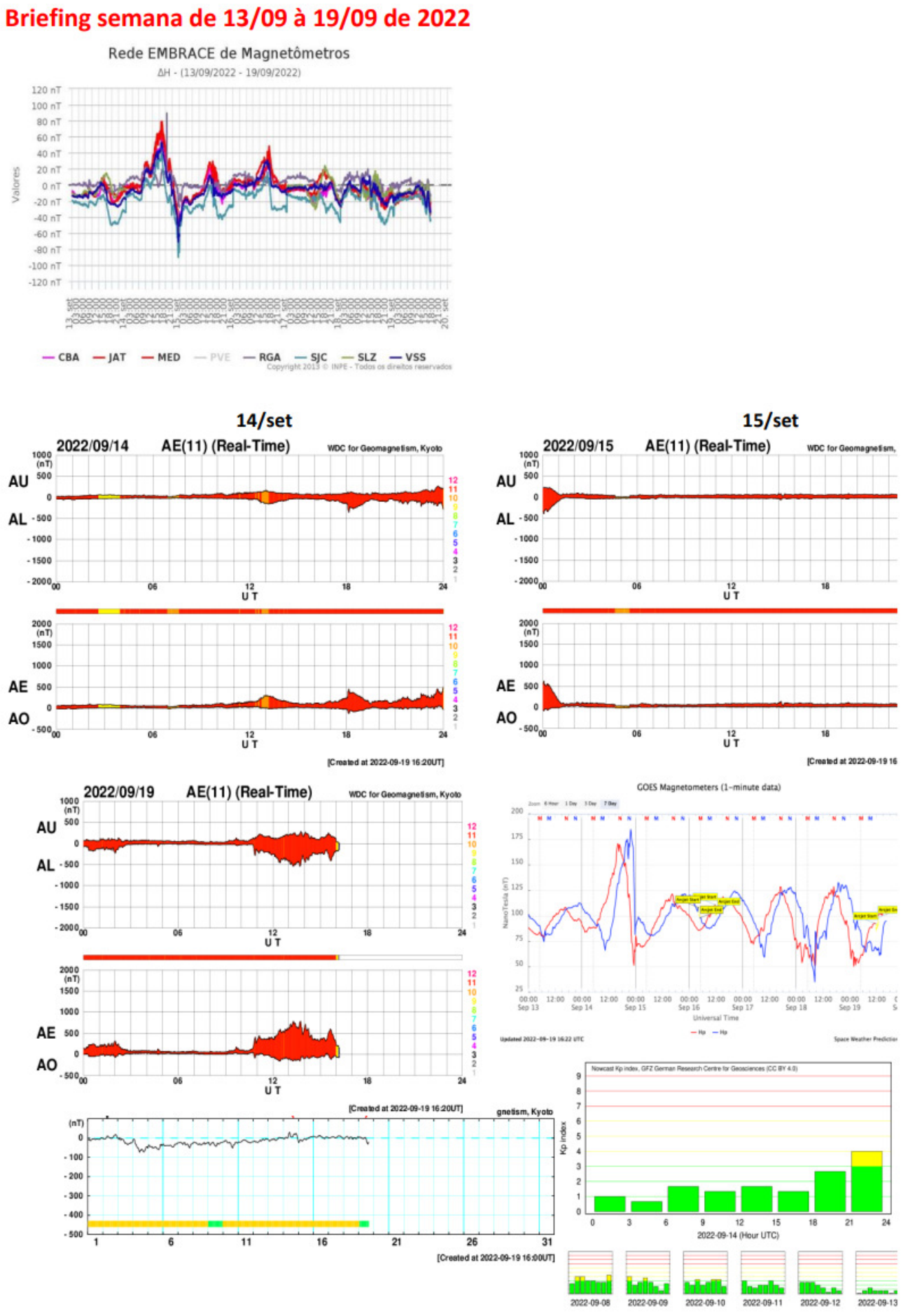

Figura 7: The figures from top to bottom show the weekly evolution of the H magnetic field component measured by the Embrace network, of the auroral AE index, of the geomagnetic field measured by the GOES satellites at $L \sim 6.6$, along with the Kp and Dst geomagnetic indices.

7 Scintilation

7.1 Responsible: Siomel Savio Odriozola

In this report on the S4 scintillation index, data from SLMA in São Luiz/MA, STNT in Natal/RN, STCB in Cuiabá/MT and SJCE in São José dos Campos/SP are presented. The S4 index tracks the presence of irregularities in the ionosphere having a spatial scale $\sim$ 360 m. Moderate to severe scintillation events were detected throughout the week in three of the four seasons analyzed (SLMA, STNT and STCB) (Figure 1). The only station that did not show scintillation measurements above 0.2 was SJCE. The most severe event occurred between 13-14/09 for STNT and between 16-17/09 for SLMA, as shown in Figure 2. This behavior from the past week confirms the start of the 2022-2023 ionospheric plasma bubble season.

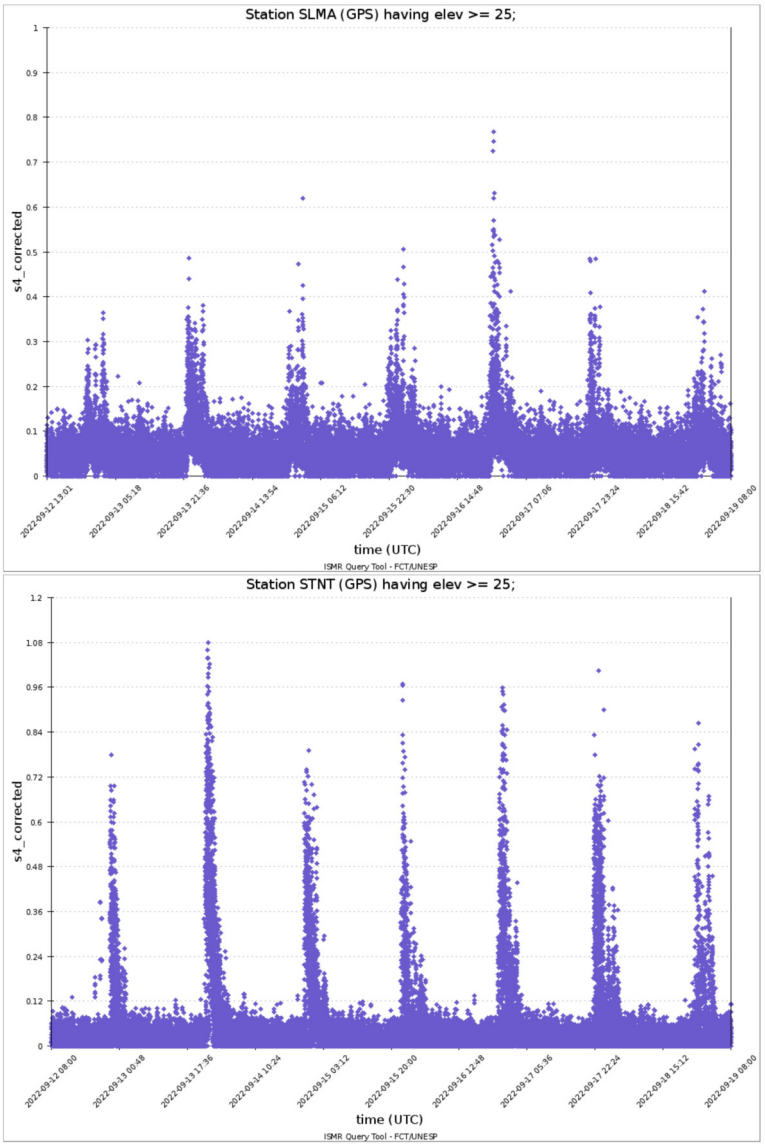

Figure 1: S4 index values for the GPS constellation measured at SLMA (upper panel) and STNT (lower panel) during the week 09/12 – 09/19.

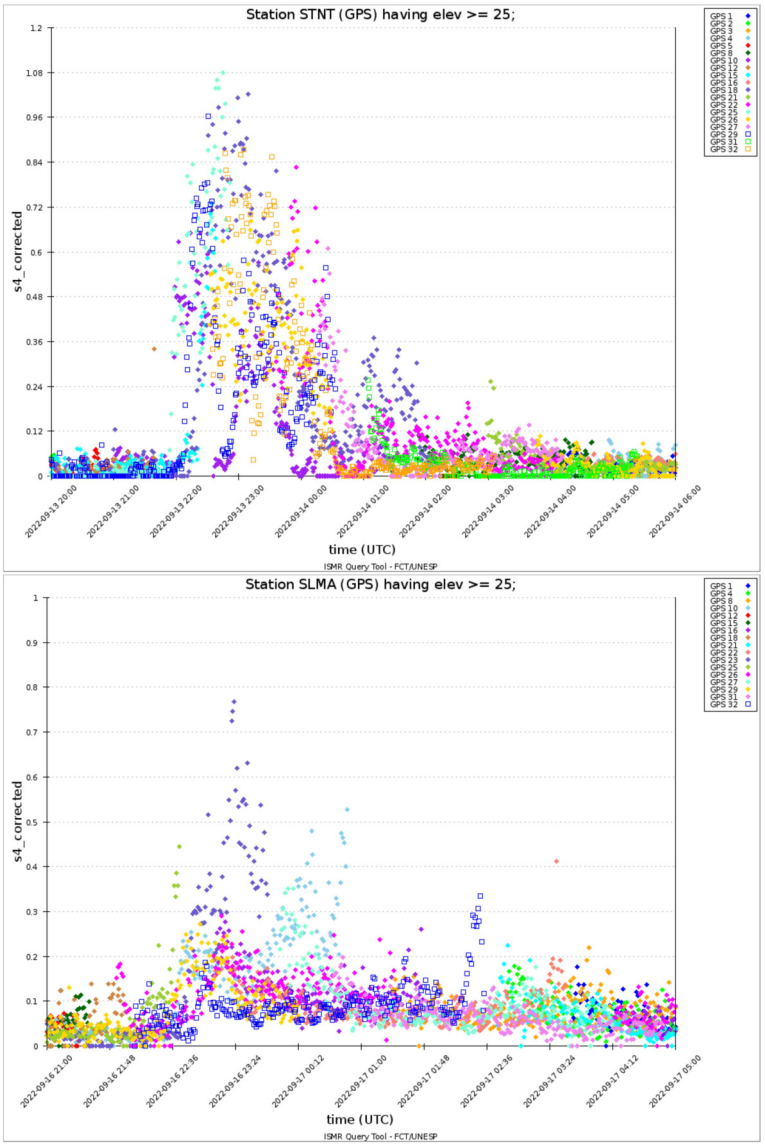

S4 index values for the GPS constellation measured at the STNT station between 20UT of the 13th to 06UT of the following day (upper panel) and SLMA between 21UT of the 16th to 05UT of the following day (lower panel).

8 ROTI

8.1 Responsible: Carolina de Sousa do Carmo

In the week 2227 (September 11 to 17, 2022) there were ionospheric irregularities (plasma bubble), on all analyzed days, as shown in Table 1. In addition, Figure 1 shows an example of the plasma bubble occurrence on September 17, 2022, using keograms at $-5°$ and $15°$ latitude.

Sunday	2022/09/11	22:30-24:00
Monday	2022/09/12	00:00-03:00; 22:30-24:00
Tuesday	2022/09/13	00:00-04:30; 22:00-24:00
Wednesday	2022/09/14	00:00-04:00; 22:30-24:00
Thursday	2022/09/15	00:00-04:00; 22:30-24:00
Friday	2022/09/16	00:00-05:00; 22:30-24:00
Saturday	2022/09/17	00:00-05:00; 22:00-24:00

Tabela 1: 17, 2022).

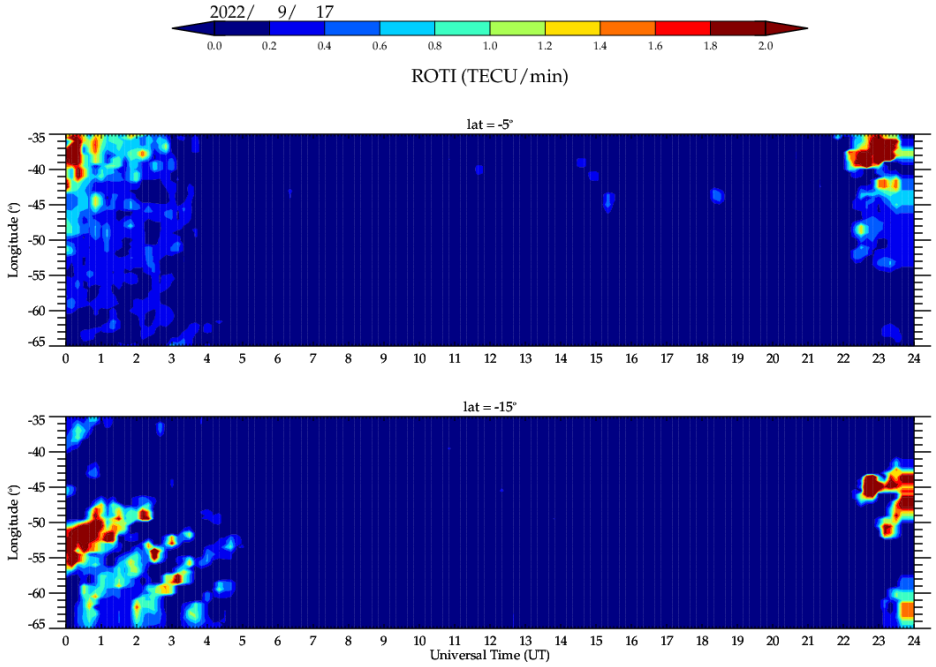

Figura 8: Keogram of September 17, 2022, for latitudes of $-5°$ and $15°$.